Calcium and synaptic dynamics underlying reverberatory activity in neuronal networks

Vladislav Volman[1,2,3], **Richard C Gerkin**[4,5], **Pak-Ming Lau**[4],
Eshel Ben-Jacob[1,2] **and Guo-Qiang Bi**[4,5]

[1] School of Physics and Astronomy, Raymond & Beverly Sackler Faculty of Exact Sciences, Tel-Aviv University, Tel-Aviv 69978, Israel
[2] Center for Theoretical Biological Physics, University of California at San Diego, La Jolla, CA 92093, USA
[3] Computational Neurobiology Laboratory, The Salk Institute for Biological Studies, La Jolla, CA 92037, USA
[4] Department of Neurobiology, University of Pittsburgh School of Medicine, Pittsburgh, PA 15261, USA
[5] Center for Neuroscience and Center for the Neural Basis of Cognition, University of Pittsburgh, Pittsburgh, PA 15213, USA

E-mail: volman@salk.edu

Abstract
Persistent activity is postulated to drive neural network plasticity and learning. To investigate its underlying cellular mechanisms, we developed a biophysically tractable model that explains the emergence, sustenance and eventual termination of short-term persistent activity. Using the model, we reproduced the features of reverberating activity that were observed in small (50–100 cells) networks of cultured hippocampal neurons, such as the appearance of polysynaptic current clusters, the typical inter-cluster intervals, the typical duration of reverberation, and the response to changes in extra-cellular ionic composition. The model relies on action potential-triggered residual pre-synaptic calcium, which we suggest plays an important role in sustaining reverberations. We show that reverberatory activity is maintained by enhanced asynchronous transmitter release from pre-synaptic terminals, which in itself depends on the dynamics of residual pre-synaptic calcium. Hence, asynchronous release, rather than being a 'synaptic noise', can play an important role in network dynamics. Additionally, we found that a fast timescale synaptic depression is responsible for oscillatory network activation during reverberations, whereas the onset of a slow timescale depression leads to the termination of reverberation. The simplicity of our model enabled a number of predictions that were confirmed by additional analyses of experimental manipulations.

1. Introduction

Persistent neuronal activity likely underlies the operation of working memory and other cellular and network functions [1–3]. The idea that reverberatory activity is maintained in neuronal circuits by virtue of recurrent excitation was first proposed by Lorente de Nó and Hebb [4, 5], and has been developed into attractor models [1, 2]. Biophysically realistic models have focused on a form of reverberation during which

neurons in the network fire in an uncorrelated fashion [2]. Although the cellular mechanisms underlying the emergence of such persistent activity in cortical networks are still being unravelled [6], the slow kinetics of the N-methyl-D-aspartate receptor (NMDAR) current has been proposed to maintain persistent activity [2], while negative feedback from slow, activity-dependent K^+ currents has been proposed to terminate it [7]. At the same time, modeling studies of spontaneous activity in developing spinal cord underscore the importance of

multiple timescale activity-dependent depression in episodic network oscillations [8].

Recently we discovered that in small networks of cultured hippocampal neurons, brief stimulation of one neuron can result in correlated, reverberatory activity persisting for seconds [9]. Using voltage-clamp recordings, rhythmic repetition of polysynaptic current events can be monitored from single neurons in the network. Typically, each event lasts for $\approx$100 ms and repeats at 5–10 Hz [9] (see also figure 2(*A*)). Such reverberatory activity is intriguing in light of the role of network oscillations in information processing and storage [10]. Mechanistically, such rhythmic reverberation may differ from the uncorrelated persistent activity studied previously [2, 11]. In particular, these reverberations are maintained primarily by amino-3-hydroxy-5-methyl-4-isoxazolepropionic acid receptors (AMPARs) and are virtually abolished by pharmacological manipulations that block asynchronous transmitter release. Asynchronous transmitter release is a fundamental property of synaptic transmission, corresponding to an increased probability of synaptic vesicle fusion that lasts for hundreds of milliseconds following an action potential due to pre-synaptic residual calcium elevation [9]. Since the rate of asynchronous release is intimately linked to pre-synaptic calcium dynamics, these results suggest that the latter might play an important role in sustaining reverberations. Importantly, in most experiments no spontaneous activity was observed, indicating that network reverberation in small cultures is likely to be mediated by synaptic, rather than intrinsic, mechanisms.

In this theoretical work, we propose a minimal biophysical model addressing the persistence and termination of rhythmic reverberatory activity as observed in small neuronal circuits. The model describes essential biophysical processes such as calcium and synaptic dynamics that may underlie reverberation, yet is controlled by a small parameter set, leading to testable predictions. We demonstrate that the emergence of rhythmic reverberatory activity can be explained by considering the dynamics of residual pre-synaptic calcium. Specifically, activity-dependent elevations of residual calcium lead to enhanced levels of asynchronous transmitter release, thus enabling a network to sustain reverberatory activity. We also show that reverberations can be terminated by a slow timescale synaptic depression. Furthermore, we associate model parameters with known biophysical processes. Thus, we can compare model behavior as these parameters change against experimental recordings obtained under corresponding changes in physiological conditions. We conclude that multiple timescale synaptic depression and the dynamics of residual pre-synaptic calcium are essential mechanisms underlying rhythmic reverberatory activity in small neuronal networks.

2. Methods

2.1. Cell culture and electrophysiology

Island cultures of dissociated rat hippocampal neurons were prepared as described previously [9]. Briefly, glass cover-slips were coated with patterns of poly-L-lysine spots ($\approx$1 mm

diameter) with custom-made rubber stamps. Dissociated cells from embryonic day 17–18 rats were plated on the cover-slips in 35 mm Petri dishes at densities of 45×10^3 to 90×10^3 cells per dish. The culture medium was DMEM (BioWhittaker) supplemented with 10% heat-inactivated bovine calf serum (HyClone), 10% Hames F-12 with glutamine, 50 units ml^{-1} penicillin/streptomycin (Sigma) and $1\times$ B-27 supplement (Invitrogen). Cultures were used at 14–21 days *in vitro* when reverberation was commonly observed in isolated networks of $\approx$50 neurons on an island of monolayer glial cells.

Perforated whole-cell patch clamp recordings were carried out with patch clamp amplifiers (Axopatch 700A, Axon Instruments) at room temperature. The pipette solution contained 136.5 mM K-gluconate, 17.5 mM KCl, 9 mM NaCl, 1 mM MgCl$_2$, 10 mM Hepes, 0.2 mM EGT and 200 g ml^{-1} amphotericin B (pH7.3). The external bath solution was a Hepes-buffered saline containing (unless otherwise indicated) 150 mM NaCl, 3 mM KCl, 3 mM CaCl$_2$, 2 mM MgCl$_2$, 10 mM Hepes and 5 mM glucose (pH 7.3). Throughout the recording, the culture was perfused with a fresh bath solution at a constant rate of $\approx$1 ml min^{-1}. Synaptic transmission in networks cultured under these experimental conditions is primarily characterized by a moderate depression (PML and GQB, unpublished observations). Polysynaptic current traces were recorded under a voltage clamp at a holding potential of -70 mV. Voltage traces were recorded under a current clamp. Stimulation pulses were 1 ms, 100 mV step depolarization (voltage clamp) or 1 ms, 2 nA current injection (current clamp) delivered at inter-stimulus intervals of at least 30 s. Signals were filtered at 2 kHz and acquired by using a 16-bit digitizing board (DigiData 3200, Axon Instruments) and processed with the pClamp software (Axon Instrument) and custom MATLAB (Mathworks) and IGOR Pro (Wavemetrics) programs. Reverberation duration was defined as the time period from the point when the rising phase of the first polysynaptic current (PSC) cluster crossed a threshold ($\approx$half of the average PSC amplitude) to the time point when the falling phase of the last PSC cluster crossed the threshold with no additional threshold crossing in the next 500 ms.

2.2. The Tsodyks–Uziel–Markram model of synaptic transmission

We begin with a simple, tractable model used by Tsodyks, Uziel and Markram to describe short-term synaptic depression (henceforth referred to as the TUM model) [12]. In the TUM model, the synaptic resource is assumed to be trafficking through any one of three possible states: recovered (X), active (Y) or inactive (Z). The equations governing the exchange of transmitter between these states are [12]

$$\begin{aligned}
\frac{dX}{dt} &= \frac{Z}{\tau_r} - uX\delta(t - t_{spike}) \\
\frac{dY}{dt} &= -\frac{Y}{\tau_d} + uX\delta(t - t_{spike}) \\
\frac{dZ}{dt} &= \frac{Y}{\tau_d} - \frac{Z}{\tau_r}.
\end{aligned} \tag{1}$$

Here, X, Y and Z are the fractions of synaptic resources in the recovered, active and inactive states, respectively. We

assume that the overall amount of synaptic resource is a conserved quantity, hence $X + Y + Z = 1$, as can be seen from equation (1). The time-series t_{spike} denote the arrival times of pre-synaptic spikes, τ_d is the characteristic decay time of post-synaptic currents (PSCs), and τ_r is the time constant of recovery from synaptic depression. Since typically cultured networks in our studies were small, we assume that there are no synaptic delays. The value of τ_d is chosen to reflect AMPAR current decay kinetics, since this post-synaptic receptor class (but not NMDARs) is critical for reverberations in hippocampal cultures [9]. The variable u describes the effective use of synaptic resources by an action potential arriving at the pre-synaptic terminal(s), and it is constant for excitatory synapses.

We assume that post-synaptic current (PSC) arriving at neuronal somata via synapses, described by equation (1), depends linearly on the fraction of available synaptic resources. Hence, an equivalent of synaptic conductance seen by a neuron is $g_{\text{syn}}(t) = AY(t)$, where A sets the scale for a density of post-synaptic effectors such as glutamate receptors.

The synaptic current entering the soma is modeled in a voltage-dependent fashion, and has the form $I_{\text{syn}}(t) = -g_{\text{syn}}(t)(V - V_r)$, where $V(t)$ is the (time-dependent) membrane voltage (exact dynamics specified below), and V_r is the reversal potential of the corresponding post-synaptic receptor type (we set $V_r = 0$ mV for AMPA receptors). Summing the pre-synaptic contributions, the total PSC entering the post-synaptic membrane of the ith neuron is

$$I_{\text{syn}}^i(t) = -\Sigma_j A_{ij} Y_{ij}(t)\left(V^i(t) - V_r^{ij}\right). \tag{2}$$

2.3. Multiple timescale depression

Synaptic dynamics are usually characterized by a diversity of timescales, endowing synapses with short-term plasticity in response to ongoing activity [13, 14]. It has also been demonstrated that hippocampal synapses utilize at least three distinct modes for vesicle recycling [14], each marked by a different timescale. To take into account the notion of multiple timescales for short-term synaptic plasticity on the phenomenological level, we extended the TUM model by introducing an additional synaptic state (called the super-inactive state). Once in the inactive state (described by Z-variable), most of the synaptic resource is directly transferred to the recovered state (X-variable), while a small fraction leaks to the super-inactive S-state, and then slowly reverts to the recovered state. During periods of elevated neuronal activity, the super-inactive state acts as a sink for synaptic resources thus providing negative feedback at a slow timescale. The trafficking of synaptic resource is shown schematically in figure 1. The augmented TUM model is thus

$$\frac{dX}{dt} = \frac{S}{\tau_s} + \frac{Z}{\tau_r} - uX\delta(t - t_{\text{spike}})$$
$$\frac{dY}{dt} = -\frac{Y}{\tau_d} + uX\delta(t - t_{\text{spike}})$$
$$\frac{dZ}{dt} = \frac{Y}{\tau_d} - \frac{Z}{\tau_r} - \frac{Z}{\tau_l} \tag{3}$$
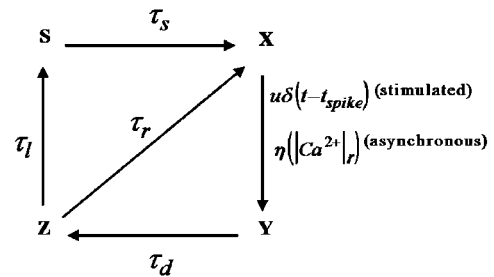$$\frac{dS}{dt} = \frac{Z}{\tau_l} - \frac{S}{\tau_s}.$$

Figure 1. Schematic representation of the model for synaptic transmission used in this work. In the model, a neurotransmitter is trafficked through four functionally distinct states. In the absence of stimulated release, some of the transmitter is spontaneously transferred from the recovered state (X) to the active state (Y), with the rate of transfer determined by the level of pre-synaptic residual calcium. After the rapid (τ_d) transition from active state to the inactive state (Z), most of the transmitter follows the direct recovery route (from Z to X within a timescale of τ_r), whilst some fraction leaks to the super-inactive state (S) within the characteristic time τ_l. From there, it recovers to the X-state on a much slower timescale τ_s. In addition to this basic route, action potentials arriving at the synapse evoke stimulated release, during which the utilized fraction of synaptic resources is determined by the parameter u.

The extent to which a super-inactive state influences persistent activity is determined by the two parameters, τ_l and τ_s, which define the characteristic time of transmitter deposition into the state and a typical time of recovery from the slow depression, respectively. As shown below, varying these parameters directly affects the duration of persistent activity in the model network.

2.4. The dynamics of residual Ca^{2+}

The basic behavior of a synapse is well captured by the above phenomenological model. However, more detailed synaptic biophysical processes often turn out to be of great importance due to their special role in the activity-dependent modulation of synaptic transmission. Upon the arrival of an action potential, the pre-synaptic terminal is depolarized, enabling calcium influx through voltage-gated calcium channels. Pre-synaptic calcium influx triggers a variety of processes, such as vesicular release of a neurotransmitter. As prolonged elevation of calcium concentration can be detrimental to cell function, there exists sophisticated machinery for calcium clearance. Most pre-synaptic free calcium is rapidly extruded through the plasma membrane to extra-cellular space [15, 16], but a small portion is taken up, at a much slower rate, by pre-synaptic organelles. The latter constitute pre-synaptic calcium stores, and complex dynamics associated with these stores have been suggested to play an important role in the regulation of synaptic function [17]. Nonetheless, after each action potential a small amount of free (not buffered) calcium is accumulated in the cytosol of the synapse. This 'residual calcium' has been postulated to affect many of the characteristics of synaptic transmission, most notably short-term synaptic dynamics and asynchronous transmitter release [16, 18].

Let us denote by $[Ca^{2+}]_r$ the concentration of residual cytosolic calcium. We also assume that the extra-synaptic concentration of calcium (formally denoted $[Ca^{2+}]_o$) is

constant. The values of $[Ca^{2+}]_o$ are on the order of mM, while a typical concentration of residual calcium is in the sub-micro-molar region [16]. The evolution of residual pre-synaptic calcium is described by

$$\frac{d[Ca^{2+}]_r}{dt} = \frac{-\beta([Ca^{2+}]_r)^n}{k_r^n + ([Ca^{2+}]_r)^n}$$
$$+ I_p + \gamma \log\left(\frac{[Ca^{2+}]_o}{[Ca^{2+}]_r}\right)\delta(t - t_{spike}). \quad (4)$$

The first term in the above equation describes the action of calcium pumps, extruding calcium from the cytoplasm back to the extra-cellular space. The second term, I_p, corresponds to passive flux of calcium into the cytosol. Finally, the third term represents the influx of calcium into the cytosol upon arrival of an action potential. This activity-dependent increase of residual calcium occurs at each action potential arrival time t_{spike}, and is driven by the electro-chemical gradient across the membrane. The parameter γ was tuned so as to result in ≈ 100 nM per spike increment of residual calcium [16]. The steady-state pre-synaptic concentration of residual calcium is therefore determined by setting the third term equal to zero (no spikes), and setting $\frac{d[Ca^{2+}]_r}{dt} = 0$. This gives $[Ca^{2+}]_{ss} = k_r\sqrt{\frac{I_p}{\beta - I_p}}$. Note that because the dynamics of calcium in the synchronous phase of transmission are much faster, the above model essentially describes only the dynamics of residual calcium.

The exponent n defines the degree of the cooperation required to activate the pump, whereas the value of k_r sets the transition from decay kinetics in the low-concentration regime to those in the high-concentration regime. For calcium extrusion pumps, the values of these parameters have been estimated as $k_r = 0.4$ μM, $n = 2$ [15]. Note also that while the maximal rate of calcium extrusion, β, is constant, the effective rate of pumping depends upon pre-synaptic calcium concentration, thus ensuring regulatory feedback.

2.5. Residual Ca^{2+} and asynchronous release

Although the exact biophysical details are unknown, evidence suggests that the relation between the rate of asynchronous release and the amount of residual calcium obeys the following Hill function [19, 20]

$$\eta([Ca^{2+}]_r) = \eta_{max}\frac{([Ca^{2+}]_r)^m}{k_a^m + ([Ca^{2+}]_r)^m}. \quad (5)$$

In the above equation, $\eta([Ca^{2+}]_r)$ is the probability of asynchronous release of transmitter (in a fixed time step), where η_{max} is the maximal rate of asynchronous transmission. The Hill exponent, m, measures the degree of cooperation required in order to activate the transmission. Higher values of m make the corresponding Hill curve steeper, and sharpen the distinction between the behavior associated with low and high calcium concentrations. Experiments performed on single synapses [19, 20] estimate the Hill exponent to be in the range $3 < m < 4$. In the simulation, we set $m = 4$. In passing, we note that such a high value of the Hill exponent (resulting in a steep threshold) seems to be an important component

for network reverberations. For smaller values of the Hill exponent ($m = 2$), less residual synaptic calcium is required to produce significant levels of asynchronous activity. This can result in dynamical instability of network dynamics, leading to spontaneous outbreaks of reverberatory activity and to the de-coordination of population dynamics (data not shown).

The threshold values of residual calcium needed to activate the asynchronous release of transmitter vary from <0.2 μM for chromaffin cells [21] to >20 μM for retinal bipolar nerve terminals [22]. This large variability across different synapses might be attributed to the existence of distinct Ca^{2+} sensors or different molecular organizations at the active zone [23]. Guided by the reported importance of asynchronous transmitter release at hippocampal synapses [9, 24], by the fact that variations as small as $\Delta[Ca^{2+}]_r \sim 100$ nM can significantly increase the frequency of release, and by the realization that the affinity for asynchronous release is evidently higher than the affinity for Ca^{2+} clearance, we propose a sub-micro-molar value for k_a, and use $k_a = 0.1$ μM in the simulations.

2.6. The enhanced (noisy) version of TUM model

With the above relations between the rate of asynchronous release and concentration of pre-synaptic free calcium, the equations of synaptic transmission are modified, and take the following form:

$$\begin{aligned}
\frac{dX}{dt} &= \frac{S}{\tau_s} + \frac{Z}{\tau_r} - uX\delta(t - t_{spike}) - X\xi \\
\frac{dY}{dt} &= -\frac{Y}{\tau_d} + uX\delta(t - t_{spike}) + X\xi \\
\frac{dZ}{dt} &= \frac{Y}{\tau_d} - \frac{Z}{\tau_r} - \frac{Z}{\tau_l} \\
\frac{dS}{dt} &= \frac{Z}{\tau_l} - \frac{S}{\tau_s}
\end{aligned} \quad (6)$$

where ξ is an amplitude of the miniature synaptic event, modeled as a random variable from a Gaussian distribution with positive mean $\langle\xi\rangle$. We assume very weak variations in the amplitude of miniature events, since these are believed to be a release of a single vesicle, but still there could be some variability in vesicle size. Such spontaneous events of stochastic amplitude are generated with the calcium-dependent rate $\eta([Ca^{2+}]_r)$. The stochastic term is added in such a way so as to satisfy the resource conservation constraint, $X + Y + Z + S = 1$. Note also that the quantity of spontaneously released resource is proportional to the quantity of recovered synaptic resource, X. Thus, the greater the recovered resource there is, the greater the effective amplitude of asynchronous release.

2.7. Neuronal model

Choosing a plausible description for neuronal dynamics constitutes an important step in the construction of model that aims to describe dynamical behavior of neuronal network. Single neuron dynamics are usually studied using detailed compartmental models [25]. This approach, however, becomes computationally expensive when large assemblies

of coupled neurons are considered. A rule of thumb is to pick a simplified description of individual neuron dynamics when large assemblies of cells are simulated, or when a detailed membrane model is believed to be not critical to the phenomena under study. As applied to the study of reverberation in the cultured networks described here, we note that (1) since reverberating activity is marked by depolarization of neuronal membrane and action potentials are of graded magnitude, the dynamics and fluctuations of membrane voltage are likely to be important; (2) studies of network dynamics and synaptic kinetics become computationally expensive, especially when longer periods of simulation (as is needed for the exploration of parametric space) are needed. Guided by the desire to retain a plausible model of neuronal dynamics, and at the same time to have at hand an efficient (from a computational point of view) system, we have chosen to describe the neuronal dynamics with a simplified two-component, single compartment Morris–Lecar model [26, 27]:

$$C\frac{\mathrm{d}V}{\mathrm{d}t} = -I_{\mathrm{ion}}(V, W) + I_{\mathrm{ext}}(t)$$
$$\frac{\mathrm{d}W}{\mathrm{d}t} = \theta\frac{W_{\infty}(V) - W(V)}{\tau_{\mathrm{W}}(V)} \tag{7}$$
$$\tau_{\mathrm{W}}(V) = \left(\cosh\left(\frac{V - V_3}{2V_4}\right)\right)^{-1}$$

with $I_{\mathrm{ion}}(V, W)$ representing the contribution of the internal ionic Ca^{2+}, K^+ and leakage currents with their corresponding channel conductivities g_{Ca}, g_{K} and g_{L} being constant:

$$I_{\mathrm{ion}}(V, W) = g_{\mathrm{Ca}}m_{\infty}(V - V_{\mathrm{Ca}}) + g_{\mathrm{K}}W(V - V_{\mathrm{K}})$$
$$+ g_{\mathrm{L}}(V - V_{\mathrm{L}}). \tag{8}$$

The current $I_{\mathrm{ext}}(t)$ represents all the external current sources stimulating the neuron, such as signals received through its synapses, glia-derived currents, artificial stimulation as well as any noise sources.

The equations for steady-state fractions of open potassium and calcium channels are

$$W_{\infty}(V) = \frac{1}{2}\left(1 + \tanh\left(\frac{V - V_3}{V_4}\right)\right)$$
$$m_{\infty}(t) = \frac{1}{2}\left(1 + \tanh\left(\frac{V - V_1}{V_2}\right)\right). \tag{9}$$

The advantage of the Morris–Lecar model is that it can easily be set to describe either type-I (saddle-node on invariant circle) or type-II (Hopf) dynamics of neuronal somata; the two types describe the two qualitatively different ways in which the transition from the quiescent to the spiking phase is accomplished [27]. Because experiments indicate that during the reverberation phase neuronal somata are depolarized and neuronal spike responses are of graded amplitude [9], we modeled the dynamics of individual neurons as type-II. While transmitter release in hippocampal neurons is coupled to sodium spikes, rather than calcium spikes, the exact form of the neuronal model is unimportant, provided that simulations of membrane potential evolution roughly match experimental data. We were able to obtain reverberatory activity in model networks using either type-II or type-I neurons, indicating that the detailed form of transition from quiescent to spiking

states is not crucial to reverberation; nonetheless, we note that model reverberations with type-II neurons better resemble those observed in hippocampal networks. Note also that although our model describes calcium dynamics in both neuronal somata and synaptic boutons, the two calcium concentrations (in soma and in synaptic bouton) are different dynamical quantities. Thus only the synaptic calcium variable is relevant for synaptic transmission, whereas the somatic calcium variable is just for controlling membrane potential dynamics as described by the Morris–Lecar model.

2.8. Network connectivity and synaptic strength

To investigate the characteristics of calcium-driven short-term persistent activity in model networks, we simulated the dynamics of a 60 neuron network. To comply with physiological data (unpublished observations), 10% of the neurons were set to be inhibitory. Next, for each pair of model neurons, we establish unidirectional synaptic connections with probability p_0. After network topology was constructed, we drew the absolute strength of synaptic connections between pairs of neurons (i, j) from a Gaussian distribution with positive mean. Completely unbounded distributions of synaptic strength are not physiologically plausible [28, 29]; in addition, with very wide distributions, a model network is likely to exhibit spontaneous outbreaks of reverberations (see the discussion). Since our primary goal in this work is to explore the characteristics of evoked reverberatory activity, we imposed boundaries on synaptic strength, retaining only the values that satisfied the localization constraint $0.8\langle A\rangle \leqslant A \leqslant 1.2\langle A\rangle$. The synaptic connectivity, the neuronal threshold and the averaged value of synaptic strength in the network were tuned according to the following heuristic principle. Because of geometrical constraints, neurons grown on isolated glial islands can develop very strong synaptic connections consisting of large numbers of boutons. In addition, experimental observations [9] indicate that a single neuron fires 0–2 spikes during the PSC cluster. Hence, we tuned the threshold and the averaged synaptic strength so as to produce one post-synaptic spike upon activation. The values of synaptic currents obtained in such a way are compatible with the estimates for hippocampal synapses [30].

Finally, because reverberations in cultured networks are robust and of finite duration even under the complete blockade of GABAergic synapses [9] we mimic this condition by nullifying the strength of all inhibitory synapses in our network. Note that even under the complete blockade of inhibition, cultured neurons in small networks fire at a moderate rate of $\sim$10 Hz during reverberation. This is much lower than the high frequency firing characteristic of paroxysmal discharges during epileptic seizure.

3. Results and discussion

3.1. The emergence of network reverberations

We begin with general observations regarding the dynamical behavior of the model network. We found that in a typical simulation (parameter choices specified in table 1)

Table 1. Parameters used in simulations.

g_{Ca}	1.1 mS cm^{-2}	V_L	-65 mV	θ	0.2	$\langle \xi \rangle$	10^{-2}
g_K	2 mS cm^{-2}	V_1	-1 mV	τ_d	10 ms	k_r	0.4 μM
g_L	0.5 mS cm^{-2}	V_2	15 mV	τ_r	300 ms	I_p	0.11 μM s^{-1}
V_{Ca}	100 mV	V_3	0 mV	τ_s	10 s	γ	80 μM s^{-1}
V_K	-70 mV	V_4	30 mV	k_a	0.1 μM	$[Ca^{2+}]_o$	2 mM
C	1 μF cm^{-2}	$\langle A \rangle$	3.41 μA cm^{-2}	n	2	m	4

the network response to brief stimulation (5 ms duration) of one neuron is characterized by the appearance of a recurrent, excitatory reverberation. This is seen clearly from figure 2(*A*) (top), in which the total post-synaptic current experienced by a sample neuron (in voltage clamp) from the model is shown. The temporal profile of the post-synaptic current resembles that observed in small networks of cultured neurons (figure 2(*A*), lower panel). Similar to the experimental results, the reverberating activity in the model network terminates after several seconds. We subsequently show that both the temporal gaps between the adjacent current clusters and the duration of network reverberation are controlled by specific biophysical parameters.

In figure 2(*B*), we show the dynamics of pre-synaptic residual calcium in the model. Each action potential invading the pre-synaptic terminal during a PSC cluster contributes to the build-up of such calcium. When a PSC cluster is terminated (due to short-term synaptic depression of evoked transmitter release), residual calcium levels are sufficiently elevated to generate abundant asynchronous transmitter release, consistent with observations in various types of synapses [31, 32]. While the concentration of pre-synaptic calcium slowly decays due to pump-related active extrusion, the fraction of synaptic resource recovered from depression simultaneously rises. At a critical point, synaptic resource recovery permits asynchronous post-synaptic current to trigger the next PSC cluster.

Reverberatory activity in the model network terminates due to the accumulation of synaptic resource in the super-inactive state (as shown in figure 2(*C*)). Thus our model demonstrates that pre-synaptic dynamics alone have the capacity to account for important features such as the initiation, continuance and eventual termination of reverberatory activity similar to that observed in networks of hippocampal neurons [9]. This conclusion is further supported by the raster plot of network activity in the model, shown in figure 3(*B*). The appearance of PSC clusters reflects the existence of short time windows during which the spiking activity of the network population is highly correlated. Note that there are no spikes in the quiescent periods between clusters, indicating that asynchronous release alone might be sufficient to provide the driving force for the initiation of the next cluster. Somatic calcium imaging data also indicate that the inter-PSC cluster periods contain few or no spikes (PML and GQB, unpublished observations).

Note that the 4-state model of synaptic resources utilized by us is crucial for persistent activity. In our model, a network has to accumulate a certain 'critical mass' of available neuro-transmitter in order to sustain its activity. Using a 3-state model (with one depression state) and a very long recovery

timescale will lead either to a failure to evoke reverberations (for strong depression), or to a transition to an asynchronous mode of activity (for weak depression). Neither corresponds to experimentally observed reverberations of finite duration.

To test how the emergence of reverberatory activity in model networks is determined by the overall synaptic strength distribution in the network, we evaluated the duration of evoked reverberations for a range of systematically varied values of the mean strength of model synapses. Figure 2(*D*) demonstrates that, for low values of mean synaptic strength, stimulation failed to induce reverberations in a model network. For higher values of synaptic strength, short reverberations (1–2 PSC clusters) were obtained. Finally, a transition to reverberations lasting for several seconds occurred slightly below the point that we used in the rest of the model simulations. Increasing the variance of the synaptic strengths (replacing the 20% constraint with the 80% constraint, i.e. using $0.2\langle A \rangle \leqslant A \leqslant 1.8\langle A \rangle$) did not lead to any qualitative changes in the profile of transition from non-reverberatory to reverberatory phases (figure 2(*D*)). These results indicate that in our model reverberation is a robust phenomenon with respect to variations in synaptic strength distributions. Meanwhile, the mean connection strength in the network plays a critical role in the emergence of reverberation, consistent with experimental observations [9].

The membrane voltage profile for a sample model neuron (figure 3(*A*), upper panel) shows that the phase of persistent network activity is characterized by neuronal membrane depolarization (driven by polysynaptic inputs). This observation is again in qualitative agreement with experimental findings (figure 3(*A*), lower panel), yet quantitatively the range of the model's membrane potential values appears to be off by a constant factor from those of cultured neurons. This discrepancy follows from model neuron selection (ML), and one might argue that selecting another model would lead to qualitatively different results. To test whether this is the case, we performed model simulations with both type-I and type-II neurons (selecting two versions of the Morris–Lecar model). For both choices, we observed network reverberation (data not shown). Hence, the choice of a particular spiking neuron model does not appear to be critical for the emergence of reverberations.

3.2. Reverberation duration in small networks is determined by the rate of slow depression and the rate of pre-synaptic calcium extrusion

Earlier studies have explored the mechanisms responsible for the existence of various types of persistent activity in large neuronal networks across different preparations. For example,
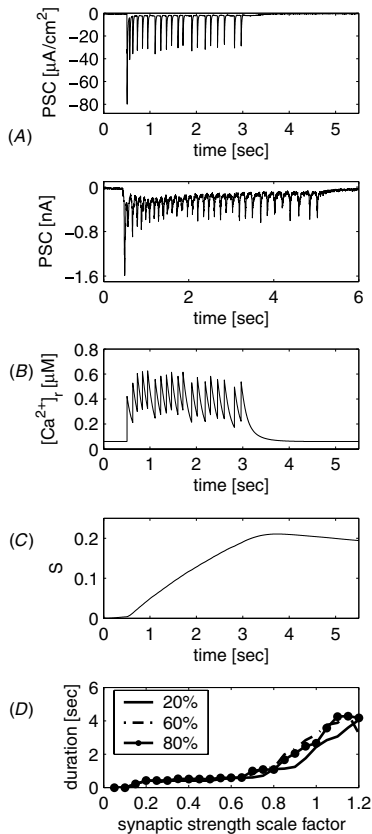
Figure 2. Activity characteristics of a model neuron. (*A*) Upper panel: a post-synaptic current (PSC) trace of a sample neuron from a model network demonstrates the emergence of reverberating activity. The activity persists for several seconds, and spontaneously terminates as a result of slow timescale depression. Lower panel: for comparison, a PSC trace recorded at a voltage-clamped neuron in a cultured network is shown to illustrate reverberatory network activity in response to a 1 ms stimulation of another neuron. As previously reported [9], this reverberatory activity takes the form of polysynaptic current clusters; each cluster lasts for ~50 ms, and the temporal gap between two adjacent clusters is ~150 ms. Note the overall similarity between the simulated and experimentally recorded traces. (*B*) Pre-synaptic residual calcium at a sample model synaptic terminal. In the absence of stimulated activity, the concentration of pre-synaptic calcium relaxes to $[Ca^{2+}]_{ss} \sim 60$ nM. Action potentials arriving at the synaptic terminal lead to the transient elevation of pre-synaptic calcium levels, with the typical values reaching 0.8 μM. This elevated calcium is responsible for the enhanced level of asynchronous release, which serves to sustain the network in the reverberating state. (*C*) During the reverberatory phase, there is a constant deposition of synaptic resource into the super-inactive depression state, from where it recovers with a very slow (several seconds) time constant. Consequently, the fraction of synaptic resource in the slow depression state eventually becomes high enough to make synaptic transmission ineffective, leading to termination of the network reverberation. (*D*) Dependence of evoked reverberatory activity on the characteristics of synaptic strength. Mean strength of model synapses has been scaled relative to the value used in the rest of the simulations. Networks with low averaged synaptic strength responded with a single PSC cluster. A transition from non-reverberatory to reverberatory phase occurred at 0.65 of the value used in simulations. Variation of constraints on strength distribution (boundaries located 20%, 60% and 80% away from mean value) led qualitatively to the same profile of phase transition. Simulations in (*A*)–(*C*) were with $\langle A \rangle = 3.41$ μA cm^{-2}, and data points were averaged over ten statistically independent realizations.
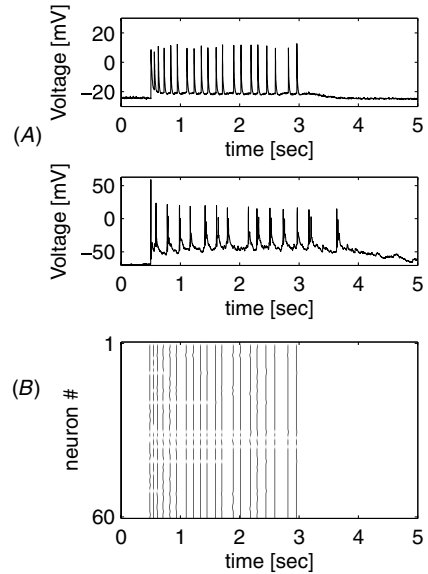

Figure 3. Membrane voltage fluctuations in a reverberatory model network. (*A*) Upper panel: membrane voltage trace of a sample neuron in the model network reveals that the neuron fires 1 spike during each PSC cluster. Between the clusters, the neuronal membrane potential fluctuates due to the enhanced levels of asynchronous release. Lower panel: sample voltage trace recorded in a current clamp from a neuron in a cultured network [9]. Reverberatory network activity is detected as membrane depolarization. During each PSC cluster, a neuron typically fires 0–2 spikes. Also, note the sub-threshold fluctuations of membrane potential between spikes. (*B*) The reverberatory behavior at the network level is reflected in a raster plot of network activity (black marks correspond to neuronal firing). The raster plot reveals that during the PSC clusters, most of the population is firing in a highly correlated manner. Hence, PSC clusters in the model network represent temporally localized events. The temporal resolution (size of each bin) is 10 ms.

spindle oscillations in a large-scale thalamic model were found to emerge from reciprocal interactions between excitatory and inhibitory populations [33]. On the other hand, the synaptic basis of cortical persistent activity is thought to be activation of NMDA receptors [2]. However, inhibition and NMDA-like excitation were shown to be not necessary for network reverberations in small hippocampal cultures [9]. Instead, the ability of a model network to exhibit reverberatory activity depends on the factors that determine the readiness of the network to generate a new PSC cluster at each time-point. Examples of such time-dependent factors are effective synaptic strength and distance to action-potential threshold. The parameters that determine whether sequential PSC clusters will continue to be generated, and that control reverberation duration, are likely to be related to underlying biophysical processes. Two prominent examples are the rate of transmitter leakage into the super-inactive state, and the maximal rate of pre-synaptic residual calcium clearance. Since the exact physiological values for these two rates are not known, we systematically varied them to investigate their effects on the duration of reverberating activity in the model network.

As figure 4 demonstrates, lowering the rate of synaptic resource leakage into the super-inactive state leads to an increase in reverberation duration. When $\tau_s < \tau_l$, the recovery
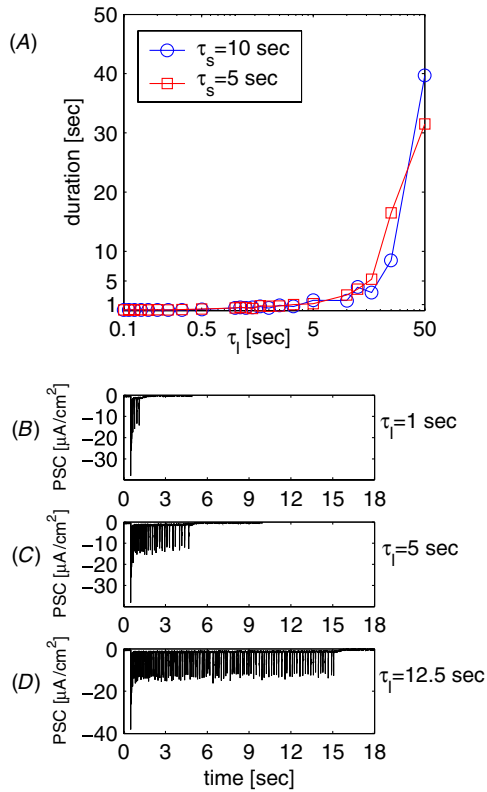
Figure 4. Dependence of reverberation duration on the rate of slow depression. (*A*) Duration as a function of the time constant of slow depression, τ_l. As the value of τ_l is decreased (for a given value of recovery time), there is a faster leak rate of transmitter into the super-inactive state, from which it recovers on a timescale of several seconds. Consequently, after a certain time the amount of resource in the recovered state is insufficient to sustain the network in the reverberating state. For high rates of slow depression the deposition rate is so fast that the activity of a network terminates after a few PSC clusters. The effect of varying the recovery time is clearly assessed when comparing the results for different values of τ_s (red curve for $\tau_s = 5$ s and blue curve for $\tau_s = 10$ s). For certain values of typical time, the networks with shorter recovery time can exhibit longer reverberations. All simulations have been performed with $\beta = 5 \times 10^{-3}$, and all data points are averaged over ten statistically independent realizations. (*B*), (*C*), (*D*) Sample PSC traces for $\tau_l = 1$ s, $\tau_l = 5$ s and $\tau_l = 12.5$ s, respectively, are shown to illustrate the qualitative dependence of reverberation duration on the rate of slow depression.

of transmitter from slow synaptic depression is fast enough to enable the network to sustain reverberation indefinitely. At the other extreme, making τ_l very rapid virtually abolishes reverberations.

We next proceeded to determine the effect of maximal calcium extrusion rate on reverberation duration. As shown in figure 5, increasing the maximal rates of calcium clearance, β, (i.e., faster effective extrusion time) decreases the rate of asynchronous release, shortening reverberation duration. However, the extent to which a calcium clearance rate can affect the duration of persistent activity is limited, because the maximal admissible duration is determined by the value of τ_l (typical time of transmitter deposition into the slow depression state).
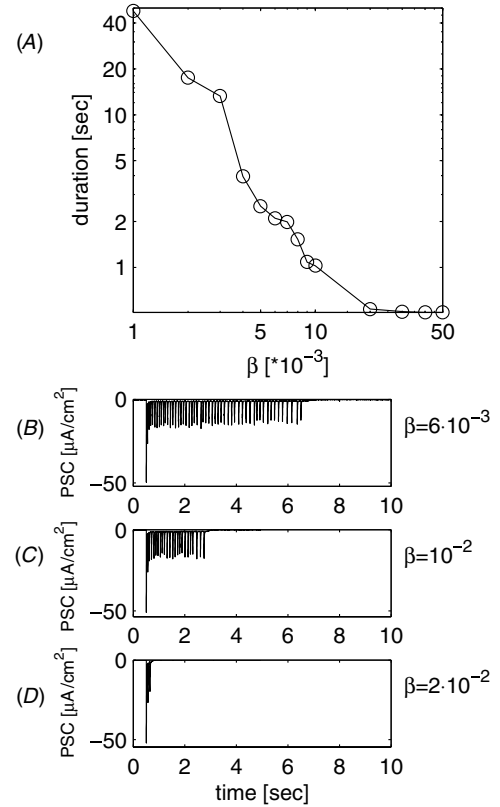
Figure 5. Dependence of reverberation duration on the maximal rate of pre-synaptic calcium clearance, β. (*A*) Duration as a function of the maximal rate of Ca^{2+} clearance. Higher values of calcium clearance are more effective at reducing the concentration of residual pre-synaptic calcium. Consequently, the levels of asynchronous release are lower, leading to earlier termination of network reverberation. (*B*), (*C*), (*D*) Sample PSC traces for $\beta = 6 \times 10^{-3}$, $\beta = 10^{-2}$ and $\beta = 2 \times 10^{-2}$, respectively, are shown to illustrate the effect of varying the value of the calcium clearance rate. All simulations were performed with $\tau_l = 5$ s, and data points were averaged over ten statistically independent realizations. Note that the actual duration of reverberation shown in (*B*) is longer than the corresponding median value (shown in (*A*)), indicating that individual realizations exhibit fluctuations (due to slightly different connectivity schemes).

3.3. Synchronous versus asynchronous release

In the model network, the sustainability of a reverberation depends on the interplay between synchronous and asynchronous release of neurotransmitter. Hence, it is of interest to study the influence of model parameters describing these two kinds of release on the emergence and characteristics of reverberations. To this end, we performed model simulations for systematically varied values of the resource utilization parameter, u, and the maximal rate of asynchronous release, η_{max} (figure 6(*A*)). The values of τ_l and β were held constant throughout these simulations, so as to fix the maximal admissible reverberation duration.

The value of the resource utilization parameter contributes to the magnitude of the post-synaptic event following the arrival of an action potential at the pre-synaptic terminal. Consequently, the resource utilization parameter is one of the factors determining the ability of a network to evoke
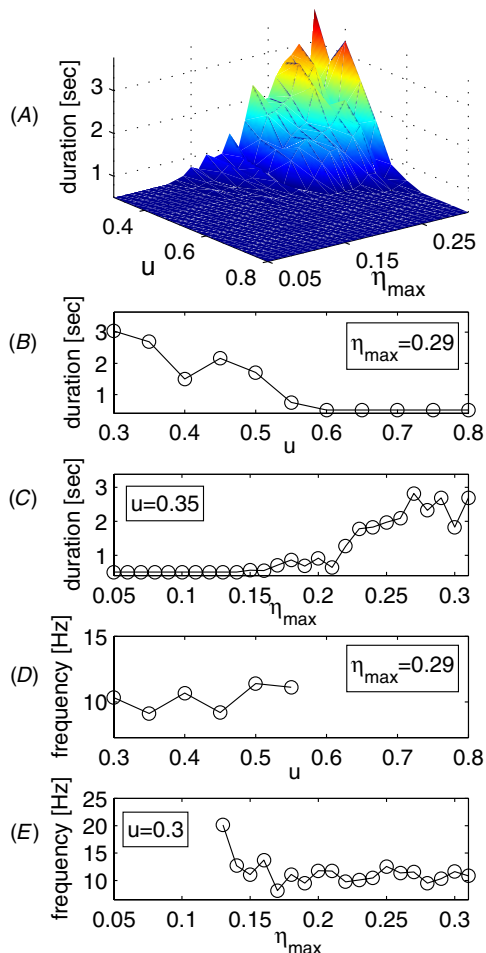
Figure 6. Dependence of reverberation characteristics on the interplay between synchronous and asynchronous transmitter release. (*A*) Duration of reverberation as a function of maximal frequency of asynchronous release η_{max}, and stimulated resource utilization parameter u. A general trend is an increase in the duration of reverberating activity as the value of η_{max} is increased, and a decrease in the duration of reverberation as the value of u is increased. This qualitative dependence on the two parameters is further demonstrated in (*B*) and (*C*) where two cross-sections of the duration surface (for constant η_{max} and constant u) are shown. (*D*), (*E*) The frequency of PSC cluster appearance depends only weakly on the maximal frequency of asynchronous release and the resource utilization parameter, consistent with experimental results (see the results). The simulations were performed with $\tau_l = 5$ s, $\beta = 5 \times 10^{-3}$ and all data points were averaged over ten statistically independent realizations.

the next PSC cluster. Low utilization of synaptic resource (small values of u) might result in insufficient excitation to generate a PSC cluster. On the other hand, high utilization can rapidly deplete the pool of transmitter, thus leading to the termination of a reverberation due to rapid accumulation of a synaptic resource in inactive states. In figure 6(*B*), we show the qualitative change in duration of reverberation as the value of u is varied. Typically, reverberation duration is inversely related to the value of u. However, below a lower critical value for u, the synchronous phase of evoked release becomes insignificant (relative to the asynchronous mode), and networks operate in an uncoordinated regime, in which

the network's activity is marked by relatively high-frequency non-coordinated neuronal discharges (data not shown).

We next evaluated the effect of varying η_{max}, the maximal rate of asynchronous release, on the duration of reverberatory activity. As shown in figure 6(*C*), increasing η_{max} typically increases the duration of a reverberation. However, when η_{max} is above a critical value, asynchronous release dominates over synchronous release, and the network again switches to an uncoordinated mode of activity (data not shown). At the other extreme, for η_{max} below a lower critical value reverberations are virtually abolished, because the level of asynchronous release is too low to provide neurons with sufficient tonic synaptic drive for subsequent PSC clusters to be generated.

The specific balance between synchronous and asynchronous release could also affect the duration of the temporal gaps between adjacent PSC clusters. To test whether this is the case, we computed the average frequency of reverberation (defined as ICI^{-1}, where an inter-cluster-interval ICI is computed as the mean interval between the peaks of adjacent PSC clusters) for different values of the resource utilization parameter u and the maximal frequency of asynchronous release η_{max}. Figures 6(*D*) and (*E*) show the trend in reverberation frequency as a function of synchronous and asynchronous release parameters. While frequency tends to increase with increasing η_{max}, the dependence is much weaker than that of reverberation duration.

3.4. Testing the model with strontium experiments

The effects of asynchronous release and pre-synaptic calcium were studied experimentally by replacing calcium with strontium in the extra-cellular medium. Strontium is known to de-synchronize transmitter release, thus enhancing the asynchronous mode of release. For experiments in which strontium partially replaced calcium, the amplitude of the current at the peak of each PSC cluster (synchronous phase) was reduced, while the amplitude of the current between peaks (asynchronous phase) was enhanced [9]. Furthermore, reverberations lasted longer. These results imply that by manipulating the 'trade-off' between the synchronous and asynchronous phases of synaptic transmission it is possible to influence the characteristics of reverberatory activity.

In the framework of the model network, strontium-induced partial suppression of stimulated synaptic transmission would correspond to a smaller value of resource utilization parameter, u. On the other hand, enhancement of asynchronous release corresponds to increasing the value of η_{max} (maximal release frequency). In order to test the predictions of the model, we made the simplifying assumption that the synchronous and asynchronous modes of transmitter release can be manipulated independently. Thus, given the approximate correspondence between model parameters and biophysical processes, we compared the experimentally observed reverberation traces under different conditions with their analogues in the model. As is seen from figure 7, these parameter changes in the model correctly reproduce the experimental effects of strontium replacing calcium. Namely, upon treatment with 'strontium', the average amplitude of the
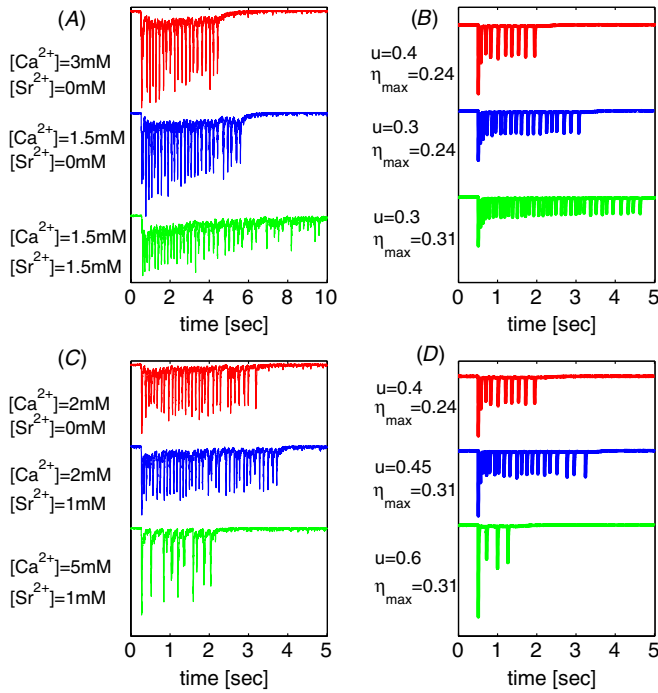
Figure 7. Generic comparison between the behavior of model and experimental networks in response to changes in ion concentrations. (*A*) Representative reverberation traces recorded from the same network under different concentrations of Ca^{2+} and Sr^{2+}—$[Ca^{2+}]$ = 3 mM, $[Sr^{2+}]$ = 0 mM (red), $[Ca^{2+}]$ = 1.5 mM, $[Sr^{2+}]$ = 0 mM (blue) and $[Ca^{2+}]$ = 1.5 mM, $[Sr^{2+}]$ = 1.5 mM (green). (*B*) Model reverberations obtained with the identification of release parameters as described in the text: $u = 0.4$, $\eta_{max} = 0.24$ (red); $u = 0.3$, $\eta_{max} = 0.24$ (blue); and $u = 0.3$, $\eta_{max} = 0.31$ (green). (*C*) Experimental traces recorded from another network under—$[Ca^{2+}]$ = 2 mM, $[Sr^{2+}]$ = 0 mM (red); $[Ca^{2+}]$ = 2 mM, $[Sr^{2+}]$ = 1 mM (blue); and $[Ca^{2+}]$ = 5 mM, $[Sr^{2+}]$ = 1 mM (green). (*D*) Model reverberations obtained for—$u = 0.4$, $\eta_{max} = 0.24$ (red), $u = 0.45$, $\eta_{max} = 0.31$ (blue), and $u = 0.6$, $\eta_{max} = 0.31$ (green). All model simulations were performed with $\tau_l = 5$ s, $\beta = 5 \times 10^{-3}$. These data illustrate that experimental alterations of the rate of both synchronous and asynchronous release dictate the properties of reverberation, and that these features are recapitulated by manipulations of the corresponding parameters in the model.

Figure 8. The effect of enhanced excitability on network activity. (*A*) Spontaneous outbreaks of reverberatory activity could be observed when the constraint on synaptic strength was relaxed. Parameters used: $u = 0.4$, $\eta_{max} = 0.28$, $\tau_l = 5$ s, $\beta = 5 \times 10^{-3}$ and $I = 14~\mu A~cm^{-2}$. Mean synaptic strength is as indicated in the table, but no constraint was used to obtain the values of absolute synaptic strength. (*B*) In a typical simulation, a brief stimulation led to reverberatory activity lasting for several seconds. Parameters used: $u = 0.4$, $\eta_{max} = 0.32$, $\beta = 4 \times 10^{-3}$, $\tau_l = 2.5$ s, $I = 14~\mu A$ cm^{-2}. Synaptic strength distribution was constrained as described in the methods. (*C*) With an elevated value of background current ($I = 15~\mu A~cm^{-2}$, other parameters are the same as in (*B*)), simulation with an otherwise identical set of model parameters resulted in the appearance of periods of uncoordinated activity.

model network's PSC clusters decreases, while the duration of reverberations is markedly increased. An increase in the concentration of calcium has the opposite effect. In addition, the model predicts that the average temporal gap between adjacent PSC clusters should decrease moderately in the presence of strontium (i.e. the frequency at which the network reverberates should grow higher) (13 Hz in 'strontium' versus 10 Hz for 'control'). Quantitative analysis of reverberation experiments indeed shows a slight increase in reverberation frequency, consistent with this prediction (6.61 ± 0.13 Hz in strontium versus 5.95 ± 0.21 Hz for controls, $p < 0.01$, Student's *t*-test).

3.5. Spontaneous outbreaks of reverberation and uncoordinated population activity

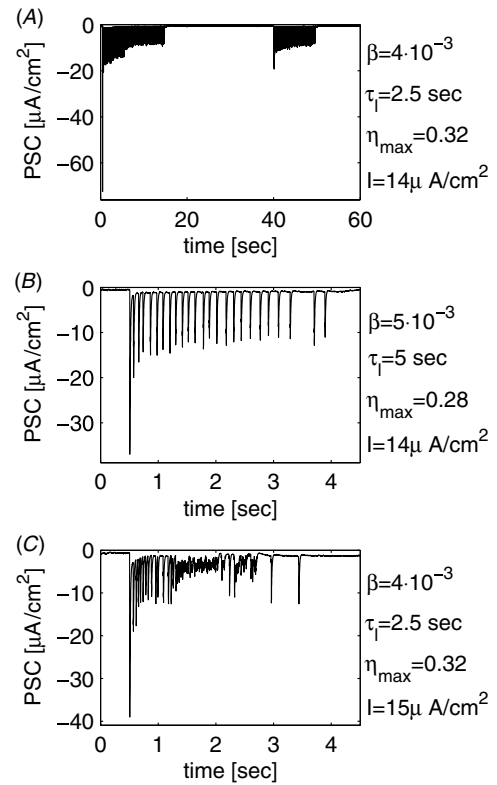Enhanced network excitability raised the chances of observing spontaneous network reverberation. When we relaxed the constraints on the variance of synaptic strength, the model network could exhibit spontaneous reverberations (in the absence of any stimulus, figure 8(*A*)). This observation can be attributed to the existence of a few very strong synaptic connections that are themselves capable of initiating the first PSC cluster of a reverberation with the help of a modest background current. Indeed, manipulations that increase synaptic strength in cultured networks can also lead to spontaneous reverberation in cultured networks (RCG and GQB, unpublished data). In model networks, we could control the appearance of reverberations by varying the relevant parameters. Normally growing networks in culture may utilize biophysical pathways to regulate their excitability in an activity-dependent manner; thus, ensuring that reverberations have the appropriate balance of rarity, PSC cluster frequency and duration. Examples of such mechanisms could be spike-timing-dependent plasticity [28], activity-dependent scaling of synaptic weights [34], or modulation from adjacent astro-glia [35]. Further research should delineate the contribution
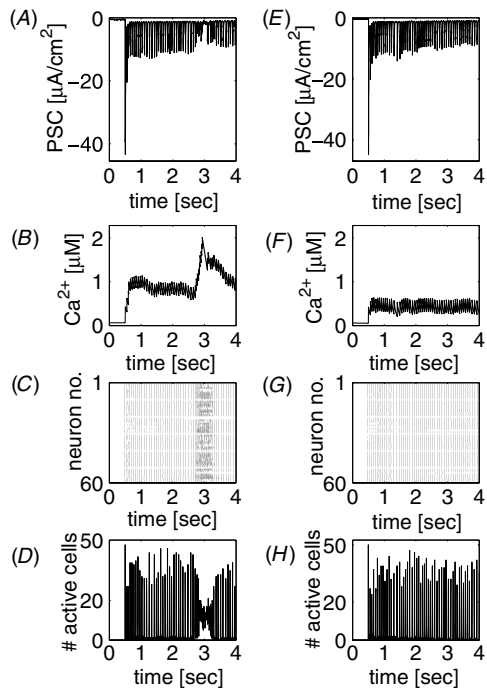
Figure 9. The generic effect of an additional low affinity calcium pump in regulating network reverberation. (A) With a single high affinity calcium pump (and without the low affinity pump), reverberatory activity can be accompanied by intermittent periods of uncoordinated activity. Such uncoordinated activity is likely to occur when asynchronous release is stronger than stimulated release (in other words, when η_{max} is high and u is low). (B) The period of uncoordinated activity corresponds to an increase in residual calcium (and a subsequent uncontrolled increase in the rate of asynchronous release). (C) Network activity during periods of high residual calcium is marked by high-rate uncoordinated discharges of model neurons (temporal resolution is 5 ms). (D) The coordination measure, defined as a number of active neurons in a time window of 5 ms. Note the dip in the number of coordinated neurons when pre-synaptic calcium is high. (E) The addition of a low affinity, high capacity pump eliminates uncoordinated outbursts. To achieve this, we have modified equation (4), as explained in the text. This modification keeps the level of residual calcium in a range that enables the network to sustain reverberatory activity. (F) The profile of pre-synaptic calcium for the synapse simulated with an additional pump. (G) Raster plot of network activity after the low affinity calcium pump is introduced into the model. (H) The coordination measure for the network augmented with an additional pump.

of these to the ability of a network to sustain healthy reverberations.

Although typically the reverberations in our model network followed the patterns of recorded activity quite well, we observed some potentially interesting distinctions between simulated and real networks. Namely, in some cases the simulated reverberations were interrupted by periods of relatively dense synaptic activity. During these windows, the electrical activity of the neuronal population was uncoordinated. Such uncoordinated behavior was not observed in cultured networks, and therefore has drawn our attention. Upon closer examination, we found that uncoordinated activity could be induced in networks with relatively elevated neuronal excitability. In addition to changes in the variance of the synaptic distribution described above,

the excitability can also be affected by a number of other parameters—for example, the value of the background current, the maximal frequency of asynchronous transmitter release, etc. As an example, elevating the value of constant background current to $I = 15$ μA cm^{-2} (instead of $I = 14$ μA cm^{-2}, as used in other simulations and as specified in table 1) led to the appearance of uncoordinated activity under otherwise 'normal' conditions, as shown in figures 8(B) and (C).

To test the idea that additional biophysical mechanisms might down-regulate these otherwise unstable network states, we modified model synapses to include an additional, high capacity low affinity calcium extrusion pump [15, 17]. Equation (4) now reads

$$\frac{d[Ca^{2+}]_r}{dt} = \frac{-\beta([Ca^{2+}]_r)^n}{k_r^n + ([Ca^{2+}]_r)^n} - \frac{0.05([Ca^{2+}]_r)^2}{4 + ([Ca^{2+}]_r)^2} + I_p$$
$$+ \gamma \log\left(\frac{[Ca^{2+}]_o}{[Ca^{2+}]_r}\right)\delta(t - t_{spike}). \quad (10)$$

Since the affinity of an additional pump is much lower than typical levels of synaptic residual calcium, it is expected to have a little effect during 'clean' reverberations. However, as seen from figure 9, the residual calcium in model synapses is rather high during outbreaks of uncoordinated activity. During these outbreaks, the number of neurons active during a narrow time window (roughly corresponding to the temporal 'localization' of PSC cluster) falls low. In this situation, the addition of a low affinity pump proves beneficial, as it can help to keep the network in the 'normal' reverberating state (figure 9).

4. Conclusion and outlook

In this work, we provide a simple yet biophysically tractable modeling framework that aims to explain the emergence, persistence and eventual termination of reverberatory activity observed in small networks of cultured neurons. Using this framework, we reproduced the salient features observed in the activity of small cultured networks—network reverberations manifested themselves in the appearance of polysynaptic current (PSC) clusters, with a typical cluster width and inter-cluster separation matching those observed in experiments. The appearance of clusters corresponded to the short periods of time during which the activity of network elements was highly coordinated.

This work also offers new insight into the mechanisms by which a network could interdigitate highly coordinated population activity with periods of silence. In order for activity to re-emerge after the silent periods, asynchronous neurotransmitter release must be sufficient to maintain the excitability of the network, while the recovery of neurotransmitter from short-term depression eventually triggers a new round of activity. This represents a biophysical implementation of the hypothesis that rapidly decaying negative feedback, combined with slowly decaying positive feedback, could maintain persistent activity in neuronal networks [36]. This may represent a general mechanism by which such networks can sustain reverberation.

Cultured networks are also known to exhibit bouts of activity called synchronized bursting events (SBEs) [37]. However, the reverberations seen here in small networks differ from the SBEs observed in large networks in at least two aspects: (a) the width of a typical SBE is larger (by a factor of 2–4) than the width of a typical PSC cluster, and (b) the separation between a pair of adjacent SBEs is several orders of magnitude larger than the inter-PSC-cluster separation. This observation hints that the mechanism underlying the generation of reverberatory phenomena in small networks differs from that responsible for the generation of SBEs in larger networks. Exactly how these mechanisms and their expression depend on network size is a question that should be resolved by further experimental and modeling studies.

It should be noted that our description of network dynamics assumes that a single action potential arriving at the synaptic terminal can evoke a spike in some of its post-synaptic targets (and generate a PSC cluster in an avalanche-like manner). Contrary to this, experiments indicate that there is a great deal of indeterminacy in neuronal responses; single stimuli were not always successful in evoking reverberatory activity [9]. Interestingly, enhanced activation of reverberation could be obtained with paired-pulse stimulation, with each pulse separated by 200–400 ms. Such paired-pulse stimuli produced greater levels of asynchronous release than one pulse alone. This observation might indicate that physiologically relevant input stimuli might drive the synapse into a resonant state with respect to pre-synaptic residual calcium dynamics, ultimately imparting the network with the level of excitability needed to sustain a reverberation.

In the present work, we have assumed that evoked synaptic transmission is 'faithful' (i.e. each incoming action potential reliably leads to transmitter release), whereas asynchronous transmitter release was modeled as a stochastic process. In reality, transmitter release is inherently stochastic; yet, due to the relatively large number of vesicles involved in evoked release in these cultures, this process might be close to deterministic. Were the variability of evoked transmitter release incorporated in our model, it would only lead to a better match with experiments (see the previous paragraph). However, such a level of description should include detailed modeling of pre-synaptic biophysics, and might become computationally much more complex for network simulations. Meanwhile, our hybrid system of deterministic evoked synaptic transmission and stochastic asynchronous release should be considered as a first approximation towards the more realistic models of calcium-driven network reverberations.

An important hypothesis concerning persistent network activity suggests that the slow kinetics of post-synaptic NMDA receptors is necessary for such activity to be sustained in an asynchronous fashion [2]. Our work, along with recent experiments [9], indicates an alternative mechanism whereby asynchronous release of neurotransmitter from pre-synaptic terminals, also with a slow kinetics, is a critical factor for the emergence of rhythmic reverberations in small neuronal circuits. It is important to note that our results do not contradict the role of NMDARs—rather, given the sustained membrane depolarization (which relieves Mg^{2+}

block of NMDARs) during reverberation, it is plausible that NMDAR activation (a post-synaptic process that is enhanced by membrane depolarization) might cooperate with asynchronous release (a pre-synaptic process that is enhanced by repeated activation) to increase the synaptic drive onto neurons during reverberations. While experimental results show that totally blocking NMDAR-mediated transmission can weaken reverberation [9], partially supporting this view, a more systematic analysis could be of interest.

Just as NMDA receptors increase network excitability, GABAergic inhibitory neurons can prevent reverberations or shorten their duration by providing negative feedback. In the present model, we have considered network reverberations in the absence of inhibition in order to delineate the importance of pre-synaptic mechanisms of recurrent excitation. In so doing, we relied on the experimental observation that in small networks normal reverberatory activity is present (and in fact enhanced) even under the complete blockade of GABAergic synapses [9]. Although beyond the scope of the current study, it is likely that in larger networks with stronger excitatory connections, inhibition plays critical roles in balancing network dynamics. In such cases, pre-synaptic residual calcium may also be important in modulating the dynamics of GABAergic transmission as well.

Our explanation of persistent activity in small neuronal circuits is based on an approximation of the biological complexity of the synapse. For example, our model incorporates only a single calcium pump, which is especially effective at clearing low Ca^{2+} concentrations. Real synapses contain many more kinds of pumps and also Ca^{2+}-storing organelles (such as mitochondria and ER). The low affinity of mitochondria for Ca^{2+} ($k_m \sim 10~\mu M$) is particularly suitable for regulation of Ca^{2+} under conditions when large influxes of calcium occur and other homeostatic processes are unable to regulate Ca^{2+} levels [17]. This would be especially relevant when a network operates in a regime of uncoordinated activity (see figure 9). More detailed models and experimental studies may ultimately elucidate the role of pre-synaptic Ca^{2+}-storing organelles in the regulation of persistent network activity. Nevertheless, our results indicate that calcium regulation at the synaptic terminal could play an important role in modulating the dynamic activity of neuronal circuits.

Acknowledgments

Glossary

Asynchronous transmission. A fundamental property of synaptic transmission, corresponding to an increased probability of synaptic vesicle fusion that lasts for hundreds

of milliseconds following an action potential due to pre-synaptic residual calcium elevation.

Synaptic dynamics.   A collective name for bio-physical processes that take place at synaptic terminals. These processes include, but are not limited to, influx of calcium into pre-synaptic terminals, release of synaptic vesicles, active extrusion of pre-synaptic calcium and refilling of synaptic vesicles.

Synaptic plasticity.   Activity-dependent changes in synaptic strength. Different forms of synaptic plasticity are distinguished on the basis of their effect (facilitation or depression) and timescale (short, intermediate or long).

Reverberation.   Self-sustained, long-lasting collective activity, generated in neuronal networks either spontaneously or in response to external stimuli.

References

[1] Durstewitz D, Seamans J K and Sejnowski T J 2000 Neurocomputational models of working memory *Nat. Neurosci.* **3** 1184–91

[2] Wang X J 2001 Synaptic reverberation underlying mnemonic persistent activity *Trends Neurosci.* **24** 455–63

[3] Marder E and Bucher D 2001 Central patterns generators and the control of rhythmic movements *Curr. Biol.* **11** R986–96

[4] Lorente de Nó R 1933 Vestibulo-ocular reflex arc *Arch. Neurol. Psychiatry* **30** 245–91

[5] Hebb D O 1949 *The Organization of Behavior—A Neurophsychological Theory* (New York: Wiley)

[6] McCormick D A, Shu Y, Hasenstaub A, Sanchez-Vives M, Badoual M and Bal T 2003 Persistent cortical activity: mechanisms of generation and effects on neuronal excitability *Cereb. Cortex* **13** 1219–31

[7] Compte A, Sanchez-Vives M V, McCormick D A and Wang X-J 2003 Cellular and network mechanisms of slow oscillatory activity (<1 Hz) and wave propagations in a cortical network model *J. Neurophysiol.* **89** 2707–25

[8] Tabak J, O'Donovan M J and Rinzel J 2000 Modeling of spontaneous activity in developing spinal cord using activity-dependent depression in an excitatory network *J. Neurosci.* **20** 3041–56

[9] Lau P-M and Bi G-Q 2005 Synaptic mechanisms of persistent reverberatory activity in neuronal networks *Proc. Natl Acad. Sci. USA* **102** 10333–8

[10] Sejnowski T J and Paulsen O 2006 Network oscillations: emerging computational principles *J. Neurosci.* **26** 1673–6

[11] Hansel D and Mato G 2001 Existence and stability of persistent states in large neuronal networks *Phys. Rev. Lett.* **86** 4175–8

[12] Tsodyks M, Uziel A and Markram H 2000 Synchrony generation in recurrent networks with frequency-dependent synapses *J. Neurosci.* **20**

[13] Hunter J D and Milton J G 2001 Synaptic heterogeneity and stimulus-induced modulation of depression in central synapses *J. Neurosci.* **21** 5781–93

[14] Gandhi S P and Stevens C F 2003 Three modes of synaptic vesicular recycling revealed by single-vesicle imaging *Nature* **423** 607–13

[15] Carafoli E 2004 Calcium signaling: a historical account *Biol. Res.* **37** 497–505

[16] Zucker R S 1996 Exocytosis: a molecular and physiological perspective *Neuron* **17** 1049–55

[17] Friel D D 2003 Mitochondrial and ER calcium uptake and release fluxes and their interplay in intact nerve cells *Understanding Calcium Dynamics* ed M Falcke and D Malchow (Berlin: Springer)

[18] Zucker R S and Regehr W G 2002 Short-term synaptic plasticity *Ann. Rev. Physiol.* **64** 355–405

[19] Ravin R, Spira M E, Parnas H and Parnas I 1997 Simultaneous measurement of intracellular Ca^{2+} and asynchronous transmitter release from the same crayfish bouton *J. Physiol.* **501** 251–62

[20] Kirischuk S and Grantyn R 2003 Intra-terminal ca^{2+} concentration and asynchronous transmitter release at single gabaergic boutons in rat collicular cultures *J. Physiol.* **548** 753–64

[21] Augustine G J and Neher E 1992 Calcium requirements for secretion in bovine chromaffin cells *J. Physiol. (London)* **450** 533–68

[22] Heidelberger R, Heinemann C, Neher E and Matthews G 1994 Calcium dependence of the rate of exocytosis in a synaptic terminal *Nature* **371** 513–5

[23] Schneggenburger R and Neher E 2005 Presynaptic calcium and control of vesicle fusion *Curr. Opin. Neurobiol.* **15** 266–74

[24] Hagler D J and Goda Y 2001 Properties of synchronous and asynchronous release during pulse train depression in cultured hippocampal neurons *J. Neurophysiol.* **85** 2324–34

[25] Segev I, Fleshman J W and Burke R E 1989 Compartmental models of complex neurons *Methods in Neuronal Modeling: From Synapses to Networks* ed C Koch and I Segev (Cambridge, MA: MIT Press)

[26] Morris C and Lecar H 1981 Voltage oscillations in the barnacle giant muscle fiber *Biophys. J.* **35** 193–213

[27] Rinzel J and Ermentrout G B 1989 Analysis of neuronal excitability and oscillations *Methods in Neuronal Modeling: From Synapses to Networks* ed C Koch and I Segev (Cambridge, MA: MIT Press)

[28] Bi G Q and Poo M M 2001 Synaptic modification by correlated activity: Hebbs postulate revisited *Annu. Rev. Neurosci.* **24** 139–66

[29] van Rossum M C W, Bi G Q and Turrigiano G G 2000 Stable hebbian learning from spike timing dependent plasticity *J. Neurosci.* **20** 8812–21

[30] Chen G, Harata N G and Tsien R W 2001 Paired-pulse depression of unitary quantal amplitude at single hippocampal synapses *Proc. Natl Acad. Sci. USA* **101** 1063–8

[31] Goda Y and Stevens C F 1994 Two components of transmitter release at a central synapse *Proc. Natl Acad. Sci. USA* **91** 12942–6

[32] Atluri P P and Regehr W G 1998 Delayed release of neurotransmitter from cerebellar granule cells *J. Neurosci.* **18** 8214–27

[33] Golomb D, Wang X J and Rinzel J 1994 Synchronization properties of spindle oscillations in a thalamic reticular nucleus model *J. Neurophysiol.* **72** 1109–26

[34] Turrigiano G G, Leslie K R, Desai N S, Rutherford L C and Nelson S B 1998 Activity-dependent scaling of quantal amplitude in neocortical neurons *Nature* **391** 845–6

[35] Angulo M C, Kozlov A S, Charpak S and Audinat E 2004 Glutamate released from glial cells synchronizes neuronal activity in the hippocampus *J. Neurosci.* **24** 6920–7

[36] Golomb D, Shedmi A, Curtu R and Ermentrout G B 2005 Persistent synchronized bursting activity in cortical tissues with low magnesium concentration: a modeling study *J. Neurophysiol.* **95** 1049–67

[37] Segev R and Ben-Jacob E 2001 Spontaneous synchronized bursting activity in 2d neural networks *Physica* A **302** 64–9